Available online at www.sciencedirect.com
ScienceDirect
Ceramics International 37 (2011) 3273–3280
CERAMICS INTERNATIONAL
www.elsevier.com/locate/ceramint

Effect of CeO_2 addition on densification and microstructure of Al_2O_3–YSZ composites

Ipek Akin, Elif Yilmaz, Filiz Sahin, Onuralp Yucel, Gultekin Goller *

Istanbul Technical University, Department of Metallurgical and Materials Engineering, 34469 Istanbul, Turkey

Received 26 April 2011; accepted 23 May 2011
Available online 27 May 2011

Abstract

Alumina (Al_2O_3) and alumina–yttria stabilized zirconia (YSZ) composites containing 3 and 5 mass% ceria (CeO_2) were prepared by spark plasma sintering (SPS) at temperatures of 1350–1400 °C for 300 s under a pressure of 40 MPa. Densification, microstructure and mechanical properties of the Al_2O_3 based composites were investigated. Fully dense composites with a relative density of approximately 99% were obtained. The grain growth of alumina was inhibited significantly by the addition of 10 vol% zirconia, and formation of elongated $CeAl_{11}O_{18}$ grains was observed in the ceria containing composites sintered at 1400 °C. Al_2O_3–YSZ composites without CeO_2 had higher hardness than monolithic Al_2O_3 sintered body and the hardness of Al_2O_3–YSZ composites decreased from 20.3 GPa to 18.5 GPa when the content of ZrO_2 increased from 10 to 30 vol%. The fracture toughness of Al_2O_3 increased from 2.8 MPa $m^{1/2}$ to 5.6 MPa $m^{1/2}$ with the addition of 10 vol% YSZ, and further addition resulted in higher fracture toughness values. The highest value of fracture toughness, 6.2 MPa $m^{1/2}$, was achieved with the addition of 30 vol% YSZ.

Keywords: A. Sintering; C. Mechanical properties; D. Al_2O_3; D. CeO_2

1. Introduction

High density sintered alumina ceramics, Al_2O_3, are widely used for orthopedic implants such as total hip and knee replacement prostheses. Their widespread use is based on a combination of good strength, high wear and chemical resistance, and good biocompatibility [1,2]. However, slow crack growth resulted in a failure of alumina ceramic component with time in service [3]. In order to increase the toughness of alumina, many techniques have been investigated based on the addition of fibers, whiskers and hard particulates.

Zirconia (ZrO_2) has been known to enhance the toughness of alumina [1]. A major drawback of zirconia ceramics is their strength reduction, due to an unfavorable tetragonal (t) to monoclinic (m) martensitic phase transformation, with time when they are in contact with physiological fluids. The t → m transform is a reversible martensitic transformation, associated with a large temperature hysteresis (around 200 °C), a finite amount of volume change (4–5%) and a large shear strain (14–15%), which leads to crumbling of the sintered part made of pure zirconia during cooling [4–6]. It has been found that zirconia shows transformation toughening mechanism that exhibits resistance to crack propagation and the transformation toughening is influenced by the grain size, the grain size distribution and the stabilizer content [4,7]. The tetragonal phase in zirconia ceramics can be obtained using yttrium or cerium oxide stabilizers. Yttria is the most popular stabilizer used for zirconia ceramics for its excellent mechanical and wear properties, and a good effect on tetragonal phase transformability [4].

Advantages of combined high hardness of alumina with highly fracture resistant yttria stabilized zirconia (YSZ) make Al_2O_3–YSZ system as an alternative choice to alumina and zirconia monolithic ceramics for structural and functional applications [1].

Similarly, hard particulates such as silicon carbide (SiC), titanium carbide (TiC) or cerium oxide (CeO_2) have been incorporated into alumina. Cerium oxide is one of the most reactive rare earth metal oxides. Due to its high oxygen storage capacity, associated with rich oxygen vacancies and low redox potential between Ce^{3+} and Ce^{4+}, high thermal stability and

* Corresponding author. Tel.: +90 212 2856891; fax: +90 212 2853427.
E-mail address: goller@itu.edu.tr (G. Goller).

0272-8842/$36.00
doi:10.1016/j.ceramint.2011.05.123

strong corrosion resistance, CeO_2 has been widely investigated in its multiple applications such as a catalyst, an electrolyte material of solid oxide fuel cells and stabilizer of several implant materials. In our previous study [8], the effect of CeO_2 addition on biocompatibility of glass ceramics was investigated. We have reported that glass ceramics having 1 wt% CeO_2 showed better cell viability. Due to its hardness and stable structure, ceria could be utilized in zirconia and/or alumina–zirconia systems [1]. Ceria is also used as a stabilizer, but in this study, it was added to the alumina matrix as a secondary phase with yttria stabilized zirconia. The results of biocompatibility tests and in vivo evaluation of Al_2O_3–ZrO_2–CeO_2 composites will be reported in another paper.

Al_2O_3 ceramics are normally densified by pressureless sintering in air or different atmospheres, resulting in a long sintering period to obtain full densification. Also, abnormal grain growth occurs during sintering process [9,10].

Spark plasma sintering (SPS) makes possible to densify Al_2O_3 based composites at a lower temperature and in a shorter time compared with conventional techniques. In the SPS technique, a pulsed direct current passes through graphite punch rods and dies simultaneously with a uniaxial pressure. The grain growth can be suppressed by rapid heating and the densification is accelerated at high temperature. Furthermore, the microstructure can be controlled by a fast heating rate and shorter processing times [11,12].

In this study, Al_2O_3 and Al_2O_3–YSZ composites containing 3 and 5 mass% CeO_2 were prepared using a spark plasma sintering method at different compositions, and densification, microstructure and mechanical properties of the samples were characterized.

2. Materials and methods

Al_2O_3 (Baikowski grade SM8, an average particle size of 0.6 μm), 3 mol yttria stabilized ZrO_2 (YSZ, Tosoh grade, an average particle size of 0.1 μm) and CeO_2 (Merck, an average particle size of 3 μm) powders were used as starting materials (Table 1). The raw materials were weighed in appropriate quantities, ball milled in ethanol for 24 h and then dried. The SEM image of the starting powder of ceria (Fig. 1(a)) showed a particle size distribution from 200 nm to ∼2 μm in diameter. The SEM image of the 90A10Z5C powder (Fig. 1(b)) revealed smaller particle size distribution of Al_2O_3, YSZ and CeO_2 at the end of the 24 h milling step.

A graphite die 50 mm in inner diameter was filled with the mixture, followed by sintering using SPS apparatus (SPS-7.40 MK-VII, SPS Syntex Inc.). Pure alumina was sintered at 1350 °C, Al_2O_3–YSZ composites with and without CeO_2 were sintered at 1400 °C for 300 s with a heating rate of 1.7 °C/s in a vacuum. A graphitic sheet was placed between the punches and the powder, and between the die and the powder for easy removal and better conductivity. A uniaxial pressure of 40 MPa and a pulsed direct current (12 ms/on, 2 ms/off) were applied during the entire SPS process. The uniaxial pressure was released during cooling for all samples.

An optical pyrometer, focused on a small hole at the surface of the graphite die, was used to measure and adjust the temperature. The current was controlled manually. Linear shrinkage of the specimens during SPS process was continuously monitored by displacement of the punch rods. The effect of thermal expansion of the graphite punch rods with increasing temperature on displacement of the specimens was negligible. The sintered specimens were in the form of pellets 50 mm in diameter and 5 mm thick and characterized after sand-blasted in order to remove the graphitic sheet.

Al_2O_3 and Al_2O_3–ZrO_2 composites without CeO_2 had a grey color at the end of the sintering process which converted to white after heat treatment. The dark coloring of spark plasma sintered composites is attributed to the carbon diffusion from the graphite sheet, dies and/or punches into the alumina. In order to remove carbon contamination, heat treatment was applied at 950 °C for 30 min in an open atmosphere. The duration of treatment was kept as short as possible to avoid grain growth. Additionally, CeO_2 is known to have different colors depending on the oxygen deficiency, such as yellow for CeO_2, blue for $CeO_{1.84}$ and blue-black for $CeO_{1.73}$ [13]. In the present study, the samples containing CeO_2 were in contact with graphite sheet, die and punch during sintering, resulting in a lower oxygen partial pressure and formation of black-yellow color at the sample surface. The presence of surrounding graphite sheet accelerated the reduction process; accordingly the surface of the sintered samples was darker. Pale yellow color was achieved after heat treatment at 950 °C for 30 min in open air furnace.

Table 1
Compositions, sintering temperatures and relative densities of spark plasma sintered specimens.

Composition	Al_2O_3 (vol%)	YSZ (vol%)	CeO_2 (mass %)	Code	Sintering temperature (°C)	Relative density (%)
Al_2O_3	100	–	–	100A	1350	99.8
$90Al_2O_3$–$10ZrO_2$	90	10	–	90A10Z	1400	99.7
$90Al_2O_3$–$10ZrO_2$–$3CeO_2$	90	10	3	90A10Z3C	1400	99.0
$90Al_2O_3$–$10ZrO_2$–$5CeO_2$	90	10	5	90A10Z5C	1400	98.8
$80Al_2O_3$–$20ZrO_2$	80	20	–	80A20Z	1400	99.6
$80Al_2O_3$–$20ZrO_2$–$3CeO_2$	80	20	3	80A20Z3C	1400	98.8
$80Al_2O_3$–$20ZrO_2$–$5CeO_2$	80	20	5	80A20Z5C	1400	99.1
$70Al_2O_3$–$30ZrO_2$	70	30	–	70A30Z	1400	99.3
$70Al_2O_3$–$30ZrO_2$–$3CeO_2$	70	30	3	70A30Z3C	1400	99.2
$70Al_2O_3$–$30ZrO_2$–$5CeO_2$	70	30	5	70A30Z5C	1400	99.3

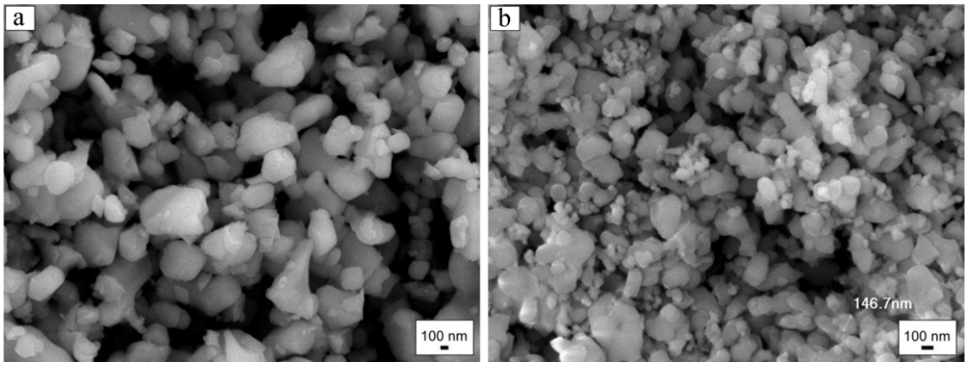

Fig. 1. SEM images of starting powder of ceria (a), and 24 h ball milled 90A10Z5C powder (b).

The bulk densities of the specimens were determined by the Archimedes' method and converted to relative density using theoretical densities of Al_2O_3 (3.97 Mg/m^3), YSZ (6.05 Mg/m^3) and CeO_2 (7.65 Mg/m^3). The crystalline phases were identified by X-ray diffractometry (XRD; MiniFlex, Rigaku Corp.) in the 2θ range of 10–80° with Cu Kα radiation. The microstructure of the starting powders and polished surfaces of the sintered specimens were observed by scanning electron microscopy (FESEM; JSM7000F, JEOL Ltd.). Vickers hardness (H_V) was measured under load of 9.8 N and fracture toughness (K_{IC}) was evaluated by a microhardness tester (VHMOT, Leica Corp.), under load of 19.6 N from the half-

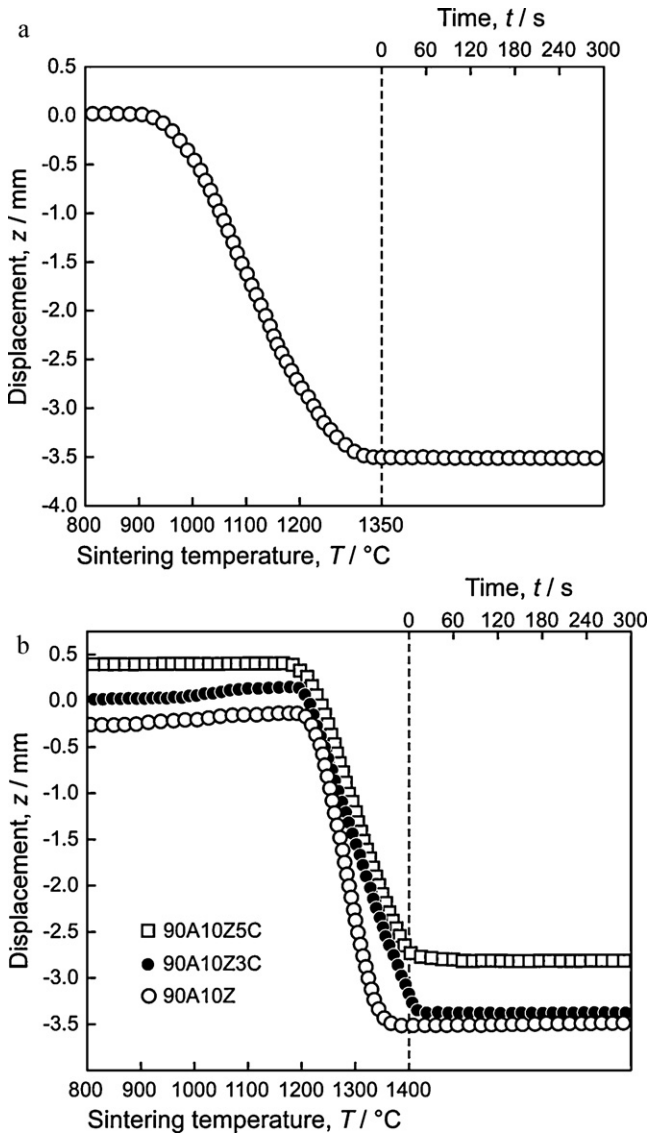

Fig. 2. Relationship between displacement and temperature and the time dependence of isothermal displacement of 100A at 1350 °C (a), 90A10Z (b), 90A10Z3C (c), and 90A10Z5C (d) composites at 1400 °C.

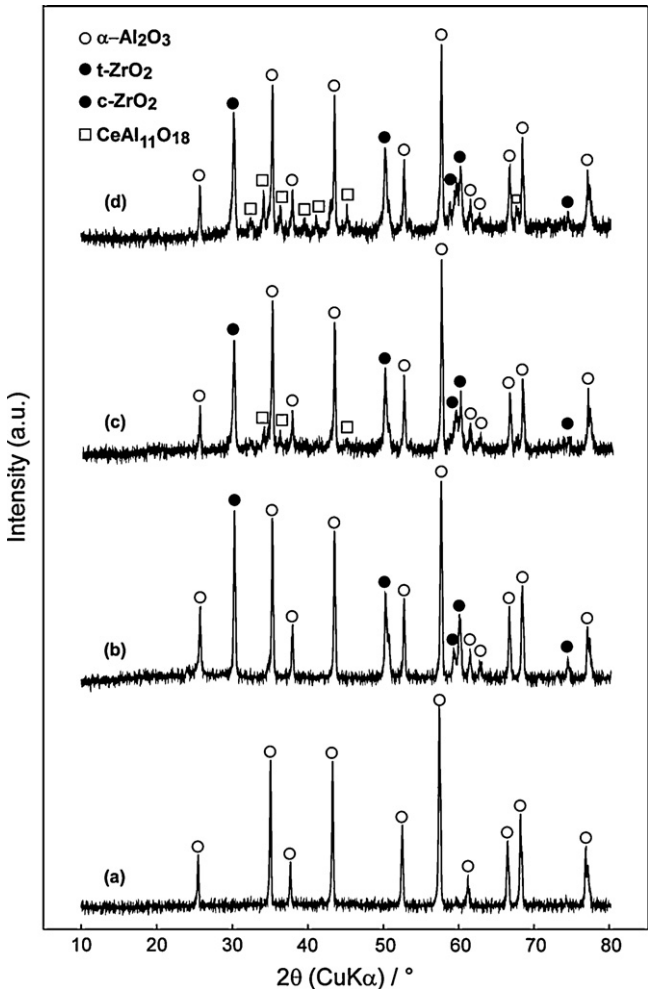

Fig. 3. XRD patterns of 100A sintered at 1350 °C (a), 90A10Z (b), 90A10Z3C (c), and 90A10Z5C (d) composites sintered at 1400 °C for 300 s.

length of a crack formed around the indentations using the following equation:

$$K_{IC} = 0.016\left(\frac{E}{H}\right)^{1/2}\left(\frac{P}{c^{3/2}}\right) \quad (1)$$

Eq. (1) was derived from Anstis et al. for median cracks. In these equations, E is Young's modulus (GPa) of composites calculated assuming a mixture rule, H is Vickers micro-hardness (GPa), P is load (N), and c is half of the average crack length [14]. The average value of the 20 measurements for each sample was used for the evaluations of hardness and toughness.

3. Results and discussion

3.1. Densification behavior and crystalline phases

The densification of the specimens during SPS process was evaluated by the displacement of punch rods due to the shrinkage of the composites. Fig. 2 shows the displacement of Al_2O_3 at 800–1350 °C and isothermal shrinkage at 1350 °C for 300 s, and Al_2O_3–YSZ composites containing 10 vol% YSZ with and without CeO_2 at temperatures of 800–1400 °C and isothermal shrinkage at 1400 °C for 300 s. The shrinkage of Al_2O_3 started at 925 °C and stopped at 1325 °C. The addition of 10 vol% yttria stabilized zirconia increased the starting and completing temperatures of shrinkage from 925 °C to 1200 °C and 1325 to 1375 °C, respectively. The addition of 3 mass% CeO_2 did not have a significant effect on the starting temperature of shrinkage of 90A10Z composite, however, shrinkage completed in 30 s at 1400 °C for the composite of 90A10Z3C. Similarly, further addition of CeO_2 resulted in same shrinkage starting temperature but shrinkage completion time increased with the addition 5 mass% CeO_2.

A relative density of approximately 99% was obtained for pure Al_2O_3 sintered at 1350 °C and Al_2O_3-based composites sintered at 1400 °C for 300 s. The relative densities (Table 1) were in agreement with the shrinkage results presented in Fig. 2.

Fig. 3 corresponds to XRD diffractions of Al_2O_3 sintered at 1350 °C, and Al_2O_3–YSZ composites containing 10 vol% YSZ with and without CeO_2 sintered at 1400 °C for 300 s. Characteristic peaks of Al_2O_3 (JCPDS: 71-1683), tetragonal zirconia (t-ZrO_2, JCPDS: 42-1164) and $CeAl_{11}O_{18}$ (JCPDS: 48-0055) were identified. XRD analysis revealed that Al_2O_3–YSZ composites containing 10 vol% YSZ with and without CeO_2 showed high tetragonal intensities of (1 1 1) planes at $2\theta = 31^\circ$ and (2 2 0) planes at $2\theta = 51^\circ$, and lower tetragonal intensities of (1 1 3) and (3 1 1) planes at approximately $2\theta = 60^\circ$. Also, the presence of low intensity (4 0 0) crystal diffraction at $2\theta = 74^\circ$ confirmed the existence of cubic zirconia (c-ZrO_2) phase [15]. No monoclinic phase of ZrO_2 was detected from the XRD results.

Since CeO_2 is easily reduced to the trivalent Ce_2O_3, formation of $CeAlO_3$ (cerium monoaluminate) and $CeAl_{11}O_{18}$ phases is possible in a reductive atmosphere. $CeAlO_3$ formation occurs by occupation of Al^{3+} cations sites Ce^{3+} after the complete reduction of CeO_2. Damyanova et al. have characterized the CeO_2–Al_2O_3 mixed oxides using different techniques and found that $CeAlO_3$ phase appears only at high reduction temperatures [16]. The characteristic peaks of $CeAlO_3$ locate at $2\theta = 33.5^\circ$, 41° and 60°. According to the XRD analysis (Fig. 3), peak formation was not observed at foresaid values. The other possible phase, $CeAl_{11}O_{18}$, was identified from its characteristics peaks at $2\theta = 34.1^\circ$ and 36.3°

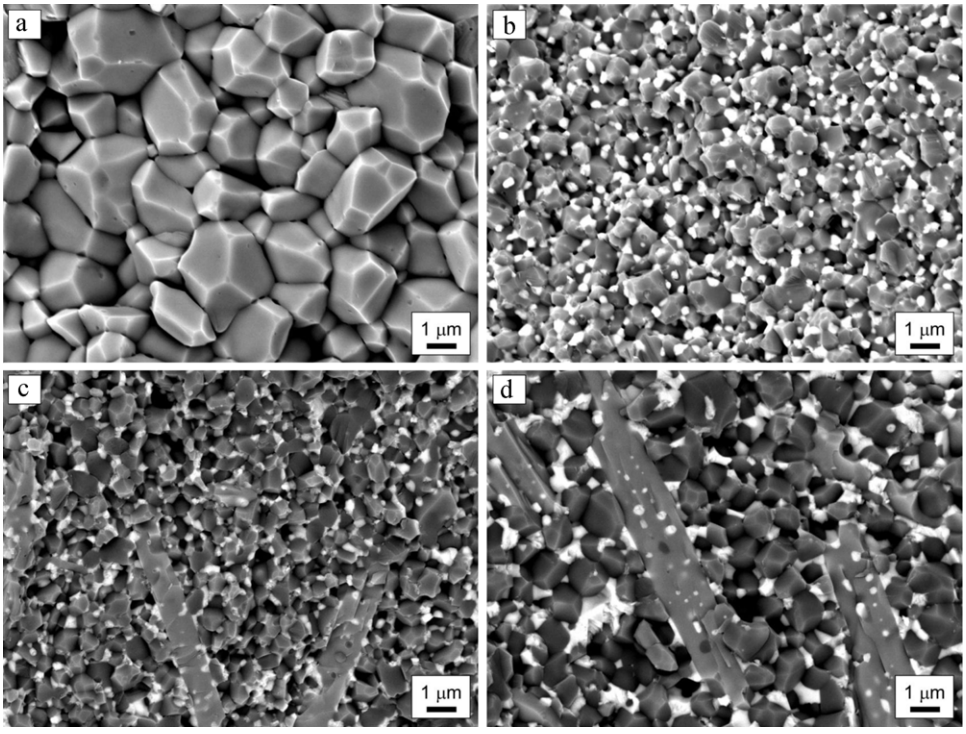

Fig. 4. SEM images of fracture surfaces of 100A sintered at 1350 °C (a), 90A10Z (b), 90A10Z3C (c), and 90A10Z5C (d) composites sintered at 1400 °C for 300 s.

(Fig. 3c and d). The formation of $CeAl_{11}O_{18}$ phase could be related to the reduction of CeO_2 to Ce_2O_3 and reaction with Al_2O_3 at higher temperatures, around 1200–1400 °C, according to the following equation (Eq. (2)) [17]:

$$Ce_2O_3 + 11Al_2O_3 \rightarrow Ce_2O_3{\cdot}Al_2O_3 + 10Al_2O_3 \rightarrow Ce_2O_3{\cdot}11Al_2O_3 \quad (2)$$

Moreover, $CeAlO_3$ is known to undergo a reversible transformation at 980 °C, $CeO_2{\cdot}11Al_2O_3$ decomposes in air between 1200 and 1400 °C [18]. So, the heat treatment that applied at 950 °C in order to remove diffused carbon from alumina matrix was low for the formation of other phases containing ceria except $CeAl_{11}O_{18}$.

Additionally, the formation of $CeAl_{11}O_{18}$ starts at 1150–1200 °C in the reductive atmosphere. The combination of shrinkage results (Fig. 2) and XRD analysis could have explained the higher shrinkage completion time of ceria containing composites [19].

3.2. Microstructural observation

Microstructures of fracture surfaces of Al_2O_3 sintered at 1350 °C and Al_2O_3–YSZ composites containing 10 vol% YSZ with and without CeO_2 sintered at 1400 °C for 300 s are shown in Fig. 4. Microstructure of monolithic Al_2O_3 consisted of both large and small equiaxed grains 0.5–3 μm in size and straight grain boundaries. Fig. 4(b) demonstrates the fracture surface of 90A10Z composite sintered at 1400 °C, where the alumina (grey) and YSZ grains (white) are shown in size of 0.6–1.5 μm and 0.05–0.1 μm, respectively. The grain growth of alumina was inhibited significantly by the addition of 10 vol% yttria stabilized zirconia. The presence of zirconia as a second phase could be beneficial with respect to inhibition of grain growth. Fine zirconia particles could have a pinning effect of grain boundaries of alumina which inhibited the grain boundary migration [20,21].

The formation of well-elongated grains of $CeAl_{11}O_{18}$ in a matrix of fine grained alumina was observed in the composites containing 3 and 5 mass% CeO_2 sintered at 1400 °C. The size of elongated $CeAl_{11}O_{18}$ grains were 5–7 μm in length and 0.8–1 μm in width, and 10–12 μm in length and 1.8–2 μm in width for 90A10Z3C and 90A10Z5C samples, respectively. The average length of elongated grains increased with increasing CeO_2 content from 3 to 5 mass% (Fig. 4(c) and (d)). It is known that, CeO_2 exhibits sensitivity to the sintering atmosphere and can form nonstoichiometric oxides such as Ce_2O_3 when sintering in vacuum, reducing or at low oxygen pressure atmosphere [22]. During spark plasma sintering process, a reducing atmosphere was created due to the high vacuum and the close contact of the powder mixture with the graphite die/punch set-up and covered sheet (Eq. (3))

$$2CeO_2 + C_{(s)} \rightarrow Ce_2O_3 + CO \quad (3)$$

CeO_2 could be reduced to Ce_2O_3 and combination with Al_2O_3 during sintering resulted in formation of $CeAl_{11}O_{18}$ ($Ce_2O_3{\cdot}11Al_2O_3$) grains during sintering. The reason of elongated shaped of them could be related to the different ionic sizes of cerium. Cerium formally has the valance 4+ in CeO_2, and 3+ in Ce_2O_3 [23]. The reduction of CeO_2 to Ce_2O_3 is associated with an increase in the ionic radius from 0.097 nm to 0.114 nm [24]. The crystal structure of $Ce_2O_3{\cdot}11Al_2O_3$ has a unit of four oxygen layers with hexagonal closed packing and one Ce_2O_3 layer, while the Al_2O_3 consists of the oxygen layers with hexagonal closed packing [17]. High cation size of ceria could have caused a distortion between layers and expanded lattice. Similar results were reported in the studies about ceria stabilized zirconia or yttria and ceria co-stabilized zirconia ceramics [25].

Fig. 5 presents the cross section microstructures of Al_2O_3–YSZ composites containing 30 vol% ZrO_2 with 3 and 5 mass% CeO_2. Fig. 5(a) and (b) clearly show that 70A30Z3C and 70A30Z5C samples had smaller grain size than that of 90A10Z3C and 90A10Z5C samples. The higher amount of YSZ could be the reason of formation of lower grain sizes due to the pinning effect. The formation of well-elongated grains of $CeAl_{11}O_{18}$ in a matrix of fine grained alumina and YSZ was also observed with a size of 0.7–1 μm in width and 10–12 μm in length, and 2–3 μm in width and 11–13 μm in length for 70A30Z3C and 70A30Z5C composites, respectively.

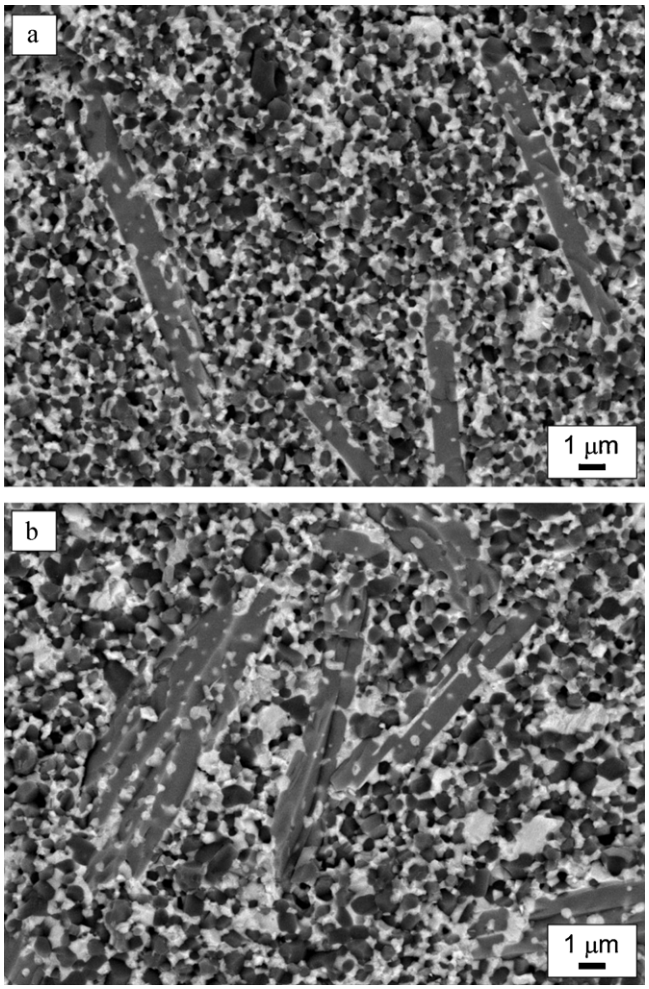

Fig. 5. SEM images of fracture surfaces of 70A30Z3C (a) and 70A30Z5C (b) composites sintered at 1400 °C for 300 s.

3.3. Mechanical properties

Fig. 6 shows the Vickers hardness of Al_2O_3 sintered at 1350 °C and Al_2O_3–YSZ composites with and without CeO_2 sintered at 1400 °C for 300 s at load of 9.8 N. Al_2O_3–YSZ composites without CeO_2 had higher hardness than monolithic Al_2O_3 sintered body and the hardness of Al_2O_3–YSZ composites decreased from 20.3 GPa to 18.5 GPa when YSZ content increased from 10 to 30 vol%. This effect could be associated with the lower hardness of 3 mol% yttria stabilized zirconia compared to that of alumina.

The hardness of Al_2O_3–YSZ composites significantly decreased with the addition of 3 mass% CeO_2 and further addition resulted in lower hardness values. This could be attributed to the formation of elongated $CeAl_{11}O_{18}$ grains (Figs. 4 and 5) due to reduction of CeO_2 to Ce_2O_3 and segregation of Al_2O_3.

The effects of composition on the fracture toughness of Al_2O_3 and Al_2O_3–YSZ composites are shown in Fig. 7. The fracture toughness of Al_2O_3 increased from 2.8 MPa $m^{1/2}$ to 5.6 MPa $m^{1/2}$ with the addition of 10 vol% yttria stabilized zirconia, and the further addition of ZrO_2 resulted in higher fracture toughness values. The highest fracture toughness,

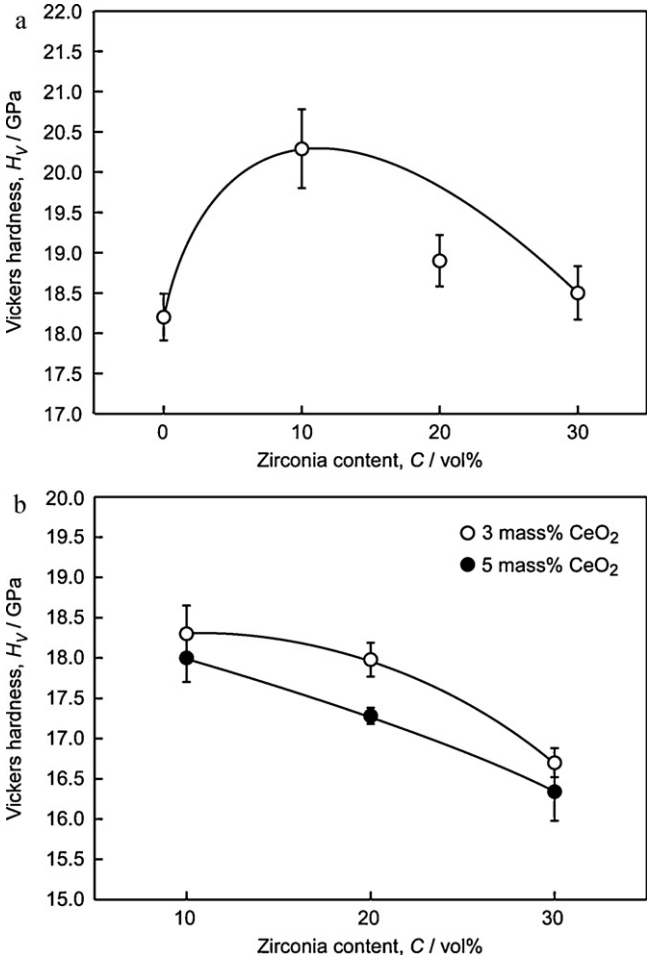

Fig. 6. Effect of zirconia content (a) and ceria addition (b) on the Vickers hardness of Al_2O_3/3Y–TZP composites.

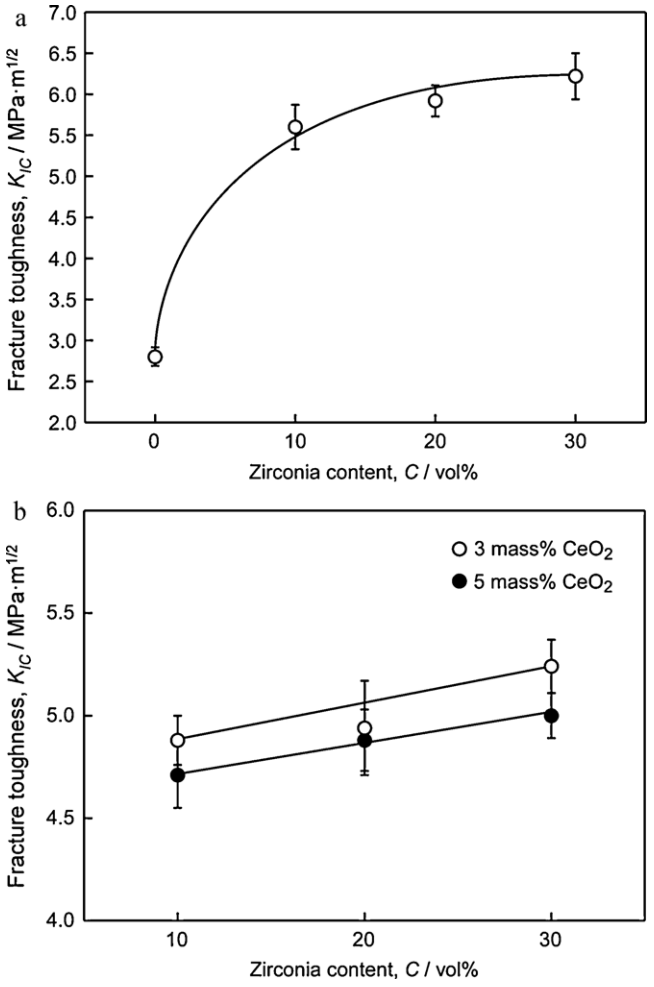

Fig. 7. Effect of zirconia content (a) and ceria addition (b) on the fracture toughness of Al_2O_3/3Y–TZP composites.

6.2 MPa $m^{1/2}$, was achieved with the addition of 30 vol% YSZ for the 70A30Z composite. The increase in the fracture toughness of Al_2O_3 and/or Al_2O_3–YSZ composites with increasing ZrO_2 content is in agreement with the previous studies. [26].

The fracture toughness of Al_2O_3–YSZ composites containing 3 and 5 mass% CeO_2 were lower than that of non-containing composites. Samples with 3 mass% CeO_2 exhibited higher fracture toughness with respect to the containing 5 mass% CeO_2 samples. Moreover, fracture toughness of the composites containing 3 and 5 mass% CeO_2 increased with increasing ZrO_2 content. This increment could be assumed to be the sum of the intrinsic toughness of the alumina matrix and the toughening mechanisms introduced by the zirconia particles such as transformation toughening, microcracking and internal stresses.

Fig. 8 shows the propagating crack of 90A10Z5C composite. The crack mode for this sample resulted in some crack deflections as indicated by white arrows with D at Al_2O_3 and YSZ phases. However, the propagated crack did not form any deflection in $CeAl_{11}O_{18}$ phases and crack directly propagated

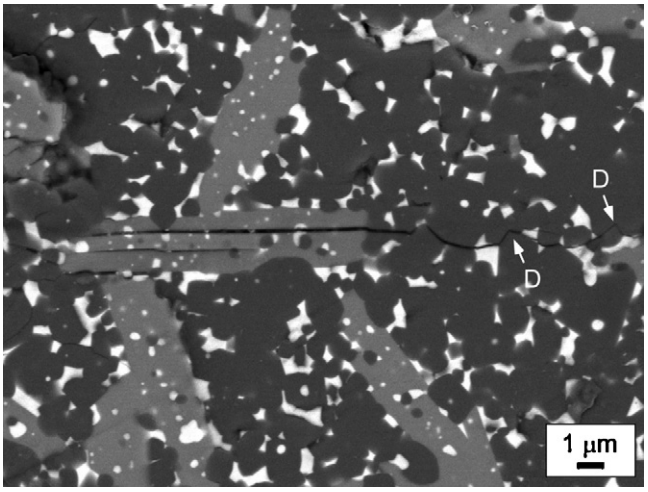

Fig. 8. SEM image of the crack propagations of the polished surface of 90A10Z5C composite.

through these grains which showed trans-granular tendency. Therefore, the fracture toughness values of the composites were prone to decrease with increasing CeO_2 content.

If these results are compared with the previously reported results [27], where the combination of maximum relative density, hardness and fracture toughness were achieved as 94.4%, 14.5 GPa and 7 MPa $m^{1/2}$, respectively, it is obvious that the results obtained in this study are superior.

4. Conclusions

Al_2O_3 and Al_2O_3–YSZ composites containing 3 and 5 mass% CeO_2 were prepared by SPS at 1350 and 1400 °C for 300 s under a pressure of 40 MPa. The results of this study showed that relative density of approximately 99% was obtained for pure Al_2O_3 and Al_2O_3–YSZ composites. The grain growth of alumina was suppressed by the addition of YSZ, and formation of elongated $CeAl_{11}O_{18}$ grains with 5–10 μm in length and 0.8–1.5 μm in width was observed in the ceria containing samples. Al_2O_3–YSZ composites had higher hardness than monolithic Al_2O_3 sintered body and the hardness of composites decreased with increasing content of YSZ. The fracture toughness of Al_2O_3 increased with the addition YSZ and the highest value of fracture toughness, 6.2 MPa $m^{1/2}$, was achieved for the composite containing 30 vol% YSZ. Formation of elongated $CeAl_{11}O_{18}$ grains resulted in lower Vickers hardness and fracture toughness values than that of the non-containing composites.

Acknowledgements

This work was supported by the Scientific Research Project Funds of Istanbul Technical University (Project Number: 33667). The authors thank H. Dincer for his contribution in SPS studies, and T.T. Alpak for SEM studies.

References

[1] N. Balagopal, K.G.K. Warrier, A.D. Damodaran, Alumina–ceria composite powders through a flash combustion technique, J. Mater. Sci. Lett. 10 (1991) 1116–1118.
[2] A.H. De Aza, J. Chevalier, G. Fantozzi, M. Schehl, R. Torrecillas, Crack growth resistance of alumina, zirconia and zirconia toughened alumina ceramics for joint prostheses, Biomaterials 23 (2002) 937–945.
[3] R. Heros, G. Willmann, Ceramics in total hip arthroplasty: history, mechanical properties, clinical results and current manufacturing state of the art, Semin. Arthroplasty 9 (1998) 114–122.
[4] M. Arin, G. Goller, J. Vleugels, K. Vanmeensel, Production and characterization of ZrO_2 ceramics and composites to be used for hip prostheses, J. Mater. Sci. 43 (2008) 1599–1611.
[5] M. Szutkowska, Fracture resistance behavior of alumina–zirconia composites, J. Mater. Process. Technol. 153 (2004) 868–874.
[6] R.H.J. Hannink, M.V. Swain, Progress in transformation toughening of ceramics, Annu. Rev. Mater. Sci. 24 (1994) 359–408.
[7] J. Chevalier, B. Cales, J.M. Drouin, Low temperature aging of Y–TZP ceramics, J. Am. Ceram. Soc. 82 (1999) 2150–2154.
[8] I. Akin, G. Goller, Effect of CeO_2 addition on crystallization behavior, bioactivity and biocompatibility of potassium mica and fluorapatite based glass ceramics, J. Ceram. Soc. Jpn. 117 (2009) 787–792.
[9] D. Jayaseelan, T. Nishikawa, H. Awaji, F.D. Gnanam, Pressureless sintering of sol–gel derived alumina–zirconia composites, Mater. Sci. Eng. A 256 (1998) 265–270.
[10] J.F. Roy, M. Descemond, C. Brodhag, F. Thevenot, Alumina microstructural behavior under pressureless sintering and hot-pressing, J. Eur. Ceram. Soc. 11 (1993) 325–333.
[11] I. Akin, M. Hotta, F.C. Sahin, O. Yucel, G. Goller, T. Goto, Microstructure and densification of ZrB_2–SiC composites prepared by spark plasma sintering, J. Eur. Ceram. Soc. 29 (2009) 2379–2385.
[12] L. Gao, H.Z. Wang, J.S. Hong, H. Miyamoto, K. Miyamoto, Y. Nishikawa, D.D.L. Torre, Mechanical properties and microstructure of nano SiC–Al_2O_3 composites densified by spark plasma sintering, J. Eur. Ceram. Soc. 19 (1999) 609–613.
[13] T. Sata, M. Yoshimura, Reduction process from CeO_2 to Ce_2O_3 in hydrogen, Bull. Tokyo Inst. Technol. 84 (1968) 13–23.
[14] G.R. Anstis, P. Chantikul, B.R. Lawn, D.B. Marshall, A critical evaluation of indentation techniques for measuring fracture toughness. I. Direct crack measurements, J. Am. Ceram. Soc. 61 (1981) 533–538.
[15] S. Yang, S. Kim, B. Kang, Y. Yun, Y. Kim, K. Hwang, Preparation of yttria-stabilized tetragonal zirconia ceramics for optical ferrule, J. Mater. Synth. Process. 9 (2001) 275–279.
[16] S. Damyanova, C.A. Perez, M. Schmal, J.M.C. Bueno, Characterization of ceria-coated alumina carrier, Appl. Catal. A-Gen. 234 (2002) 271–282.
[17] K. Tsukama, Conversion from β-$Ce_2O_3 \cdot 11Al_2O_3$ to α-Al_2O_3 in tetragonal ZrO_2 matrix, J. Am. Ceram. Soc. 83 (2000) 3219–3221.
[18] L.I. Podzorova, A.A. Il'icheva, N.A. Mikhailina, V.Y. Shevchenko, L.I. Shvorneva, Effect of preparation conditions on the phase composition of ZrO_2–Al_2O_3–CeO_2 powders, Inorg. Mater. 38 (2002) 1455–1461.
[19] D.E. Angove, N.W. Cant, D.H. French, K. Kinealy, The effect of temperature on a ceria–alumina–baria cordierite monolith combination under oxidizing and reducing conditions, Appl. Catal. A-Gen. 194 (2000) 27–34.
[20] D.J. Green, Critical microstructures for microcracking in Al_2O_3–ZrO_2 composites, J. Am. Ceram. Soc. 65 (1982) 610–614.
[21] B. Kibbel, A.H. Heuer, Exaggerated grain growth in ZrO_2-toughened Al_2O_3, J. Am. Ceram. Soc. 69 (1986) 231–236.
[22] J.Z. Shyu, W.H. Weber, H.S. Gandhi, Surface characterization of alumina-supported ceria, J. Phys. Chem. 92 (1988) 4964–4970.
[23] N.V. Skorodumova, S.I. Simak, B.I. Lundqvist, I.A. Abrikosov, B. Johansson, Quantum origin of the oxygen storage capability of ceria, Phys. Rev. Lett. 89 (2002) 166601–166611.
[24] T.C. Huang, E. Moran, A.I. Nazzal, J.B. Torrance, P.W. Wang, Determination of the average ionic radius and effective valence of Ce in the

$Nd_{2-x}Ce_xCuO_4$ electron superconductor system by X-ray diffraction, Phys. C: Supercond. 159 (1989) 625–628.

[25] S.G. Huang, K. Vanmeensel, O. Van der Biest, J. Vleugels, Influence of CeO_2 reduction on the microstructure and mechanical properties of pulsed electric current sintered Y_2O_3–CeO_2 co-stabilized ZrO_2 ceramics, J. Am. Ceram. Soc. 90 (2007) 1420–1426.

[26] R. Langlois, K.J. Konsztowicz, Toughening in zirconia-toughened alumina composites with non-transforming zirconia, J. Mater. Sci. Lett. 11 (1992) 1454–1456.

[27] R.V. Mangalaraja, B.K. Chandrasekhar, P. Manohar, Effect of ceria on the physical, mechanical and thermal properties of yttria stabilized zirconia toughened alumina, Mater. Sci. Eng. A 343 (2003) 71–75.